Modelling the morphological response of the Oka estuary (SE Bay of Biscay) to climate change.

Roland Garnier[1*], Ian Townend[2], Manu Monge-Ganuzas[3], Iñaki de Santiago[1], Pedro Liria[1], Aritz Abalia[1], Irati Epelde[1], Andrea del Campo[1], Guillem Chust[1], Mireia Valle[1], Manuel González[1], Julien Mader[1], Mariluz Gómez[4], Carlos Castillo[4], Adolfo Uriarte[3]

[1]AZTI Marine Research, Basque Research and Technology Alliance (BRTA), 20110 Pasaia, Spain

[2]School of Ocean and Earth Science, University of Southampton, Southampton SO17 1BJ, UK

[3]Natural Heritage and Climate Change Directorate, Basque Government, 01010 Vitoria-Gasteiz, Spain

[4]Ihobe, Basque Government, 48011 Bilbao, Spain

*Corresponding author: Roland Garnier, AZTI Marine Research, Basque Research and Technology Alliance (BRTA), Herrera Kaia. Portualdea z/g, 20110 Pasaia, Spain. rgarnier@azti.es

ABSTRACT

Adaptation in and around estuaries, to ensure the future resilience of both the natural environment and the communities that are located alongside is an increasingly pressing need. As part of an adaptation planning program for the Basque estuaries (northern Spain, south-eastern Bay of Biscay), a modelling system to simulate the morphological response of the Oka estuary to climate change has been developed. Existing knowledge was used as the basis to frame this pilot modelling examining both the short-term change (storm, seasonal, annual) and the longer-term changes (decades to eons). In this paper, we focus on the long-term response and consideration of the output from the process model is limited to the data that was extracted to help parameterize the long-term model. The latter was then used to examine the response of the estuary to the past changes over a historical time scale, where observations from foraminiferal analysis and saltmarsh response were used to establish the predictive validity of the model.

Forcing the model with a linear rate of sea level rise representative of the 20th century, the estuary keeps pace with sea level rise in agreement with the observations. An 18.6-year periodic variability was identified over the saltmarshes, by including the effect of the nodal tide, with the last deposition maximum occurring in 2020.

The effect of the opening of a saltmarsh that was drained at the beginning of the 18th century was investigated using a simplified schematization and showed sedimentation rates of up to one order of magnitude larger than in natural marsh, in general agreement with the rates obtained in previous studies.

To predict the future response of the estuary, simulations with an exponential sea level rise were performed using scenarios obtained from the latest IPCC projections. The estuary fails to keep pace with sea level rise in any of the scenarios considered. The

attendant increase in the hydroperiod over the saltmarshes is also likely impact to saltmarsh species productivity and distribution.

Despite the simplifications inherent to the model, and the simplifications made in the representation of the estuary and forcing conditions, the methods presented here provide additional insights into long-term behaviour that complement information obtained from more detailed, but short-term, process models. The combined modelling approach allows adaptation measures to climate change to be considered over longer timescales.

Keywords

Estuarine morphodynamics, Saltmarsh, Sea level rise, Adaptation to Climate Change, Delft3D, ASMITA.

1 INTRODUCTION

Climate change poses an increasing and unavoidable threat to estuaries around the world (Elliott et al, 2019). The Intergovernmental Panel on Climate Change (IPCC, 2021), highlighted scenarios of global sea level rise higher than previous assessment reports. In the coming decades, coastal systems and low-lying areas will increasingly experience adverse climate-related impacts (IPCC, 2021) exacerbated by increasing human-induced pressures (Wong et al., 2014) and by the historic alteration and degradation (Halpern et al., 2019). Concern about the negative repercussions derived from the loss of biodiversity and ecosystem functions of these habitats has triggered the development of conservation frameworks worldwide (IPBES, 2019). Under this context, assessing progressive adaptation strategies to ensure the future resilience of the both the natural environment and the communities that are located alongside the estuaries, has become an increasingly pressing need (Hall et al, 2019; Townend et al, 2021). To address these issues, local adaptation planning is needed but it is still in its infancy (Reiblich et al., 2019). In northern Spain, the Basque Government has initiated a research programme to develop an approach that can be applied to all the estuaries in the Basque country. To this end, the Oka estuary was selected as the pilot site because of its importance as a UNESCO Biosphere Reserve and the body of data that already exists from previous studies (Monge-Ganuzas et al., 2019). The requirement was to identify a work programme that can provide a robust evidence base (Shaxson, 2005) to support future adaptation planning and management of these estuaries.

The focus of the study was to simulate the morphological response of the Oka estuary to climate change. This would then be used to assess how habitats and communities around the estuary might be impacted over the coming century. An initial phase focused

on synthesizing the existing knowledge and evaluating various data sets to develop a conceptual model of the short-term processes that underpin the long-term changes (up to Holocene timescale) that have been recorded using an array of different techniques (Townend, 2004). This understanding was then used as the basis for framing a modelling exercise to provide further insight into both the short-term change (storm, seasonal, annual) and the longer-term changes (decades to eons). In selecting the models, careful consideration was given to the primary time-scale of the model and its suitability for the time and space scales of interest (Murray, 2007, 2013; Larsen et al, 2016; French et al, 2016, van Maanan, 2016). There are many process-based models available to study the influence of waves, winds, tides, salinity, and the associated morphological response that have been demonstrated to work well over relatively short timescales (Roelvink and Reniers, 2012, Monge-Ganuzas et al., 2017) but also been applied to examine decadal scale change (van dee Wegen & Roelvink, 2012; Dam et al, 2016). In this study we make use of the Delft3D modelling suite (Lesser et al, 2004).

An alternative approach has been to use models that aggregate the short-term processes to capture the long-term change. One such model tracks the exchange of sediment between morphological elements, relative to an equilibrium condition, and any response to perturbations in system forcing conditions. The concept referred to as the ASMITA model (Aggregated Scale Morphological Interaction between Tidal basin and Adjacent coast, Stive et al, 1998) has been shown to be entirely consistent with more detailed process models in terms of the underlying physics but with an integration timescale that is more consistent with long-term change (decades and longer, Wang et al, 2020). Recent extensions of the model also mean that processes such as littoral drift and riverine fluxes can be accounted for. In addition, the introduction of a simple bio-

morphological model to represent saltmarsh behaviour has extended the range of geomorphological elements that can be included, greatly improving the ability to represent the sort of conceptual model that frequently characterizes temperate latitude estuaries (Townend et al., 2016a). The estuaries of the Basque country are characterized by ebb and flood deltas linked by channels and flanked by extensive delta flats, with an inner estuary comprising both flats and saltmarshes either side of the main tidal channel that extends up valley to the riverine input.

Following a summary of the study site and the existing conceptual understanding of the dynamics at a range of timescales, we outline the two models that underpin the examination of morphological change. In this paper, we focus on the long-term response and consideration of the output from the process model is limited to the data that was extracted to help parameterize the long-term model. The latter was then used to examine the response of the estuary to the past changes over a historical time scale, where observations from foraminiferal analysis and saltmarsh response were used to establish the predictive validity of the model. This provided a robust basis for assessing the response of the estuary to projected sea level rise and inform the adaptation planning work.

2 STUDY SITE

The Oka estuary is located in the south-eastern Bay of Biscay in the Spanish Basque Country and belongs to the Urdaibai Biosphere Reserve declared by UNESCO in 1984 (Fig. 1). The estuary is a drowned fluvial valley composed by shallow intertidal sandy and muddy flats and saltmarshes and is tidally dominated (Monge-Ganuzas et al., 2019). Waves are a dominant influence on the enclosing spit and the ebb tidal delta. The spit is

the Laida beach, which regularly faces erosion problems and lack of available supratidal beach area (Monge-Ganuzas et al., 2017; Gainza et al., 2019). The ebb delta is formed by the Mundaka sand bar, a worldwide recognized surfing spot, whose morphology is the result of the morphodynamic interactions between the beach, the inlet, and the inner estuary. In particular, it has been seen that a perturbation to the estuary system can affect the shape and stability of its morphological elements, and can have bad repercussions on the quality of the Mundaka waves (Monge-Ganuzas et al., 2008; Liria et al., 2009). The processes that govern the morphological changes of the Oka estuary are complex and are influenced by the combined effects of tides, waves, river and wind. Moreover, several elements that have different response times interact. Predicting the response of the estuary to the future climate is a challenge that should start from the understanding of the present and past dynamics.

Sedimentary studies have shown that the estuary has progressively infilled and migrated landward over the Holocene (Cearreta & Monge-Ganuzas, 2013). At the same time, the inner saltmarshes have built up (Benito & Onaindia, 1991) due to the fluvial sediment supply (Prego et al., 2008, Peraza-Castro et al., 2015). Foraminiferal analysis and dating from sediment cores provide information on the rate of sediment deposition over the saltmarshes at Holocene (Cearreta & Monge-Ganuzas, 2013) and historic (Cearreta et al., 2013) time scales. Thanks to these studies, data of long-term morphological evolution of the Oka estuary are available, allowing the effect of past climate changes on the estuary to be examined (García-Artola et al., 2015). Moreover, the effect of human interventions in the middle and upper estuary can be quantified. Most of the saltmarshes were drained at the beginning of the 18th century for agricultural purposes and malaria eradication and subsequently abandoned during the middle of the 20th

159 century due to rural migration to the cities (Cearreta et al., 2002). Borehole analysis
160 allows us to determine the rate of accretion for natural saltmarshes (García-Artola et al.,
161 2015), but also for saltmarshes that are in the process of regeneration and have
162 experienced rates of up to one order of magnitude larger than natural saltmarshes
163 (Cearreta et al., 2013, García-Artola et al., 2015).
164
165 The observed rates of sedimentation over the saltmarshes of the Oka estuary provides a
166 source of information to calibrate and validate morphological evolution models. Up to
167 now, the existing modelling studies of the Oka estuary have focused on the
168 hydrodynamics (Monge-Ganuzas et al., 2008, 2013, 2015; Liria et al., 2009), and the
169 short-term morphological evolution: including the response to changing sea level
170 conditions (Valle et al., 2014), and the evolution at daily or monthly scale (Monge-
171 Ganuzas et al., 2017; Gainza et al., 2019) to understand the effect of dredging/dumping
172 in isolated elements of the estuary. These studies were performed with 2DH hydro-
173 sedimentary numerical models that have shown their limitation to simulate long-term
174 evolution and to aggregate elements that behave with different time scales (Coco et al.,
175 2013).
176

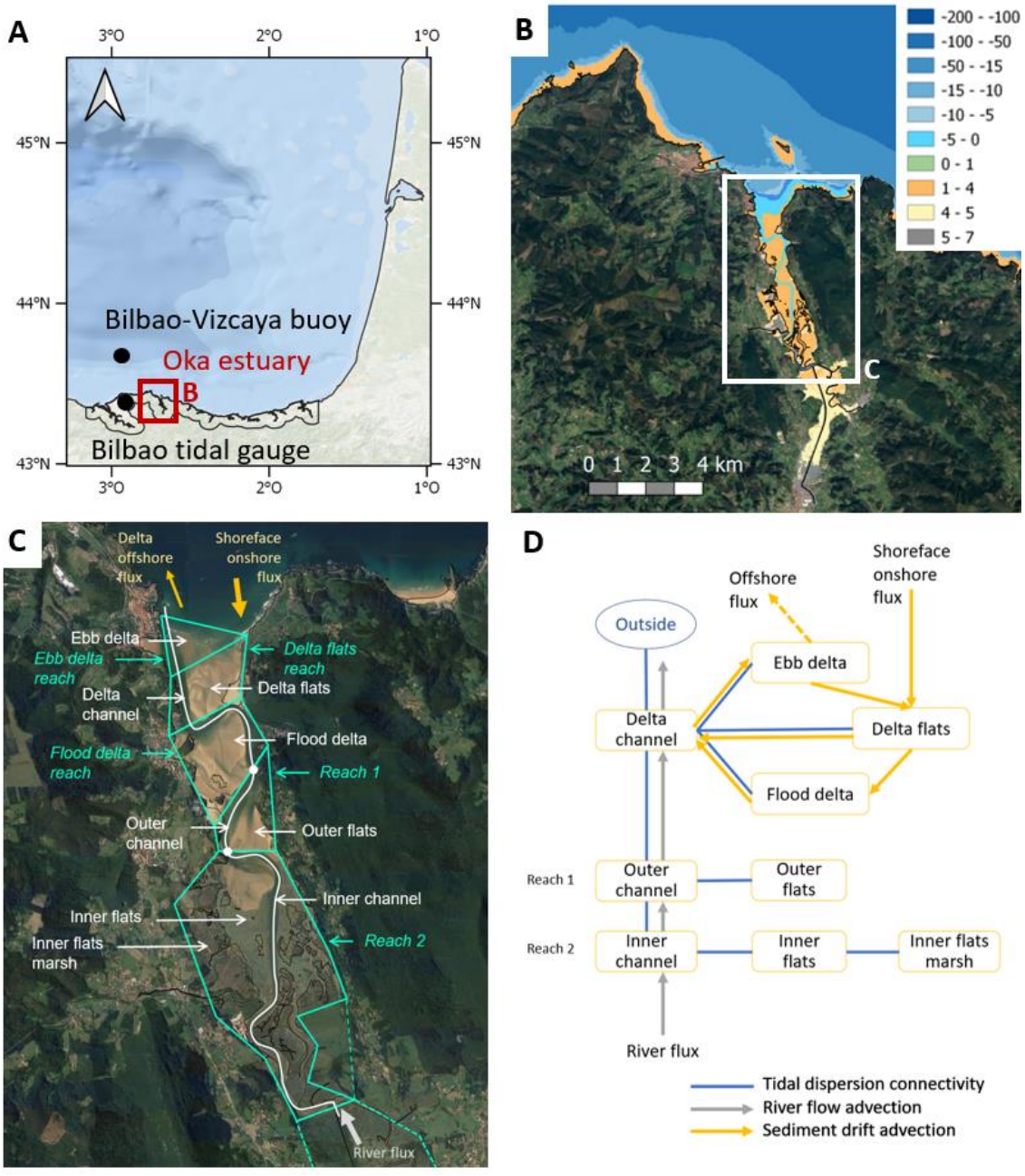

177

178 Fig. 1. Study area and morphological element schematisation. A: location of the Oka
179 estuary (red box) within the Bay of Biscay. B: bathymetry of the Oka estuary and
180 location of the domain of study (white box), the colours indicate the bottom level with
181 respect to the Bilbao port datum (in m). C: discretization of the estuary into reaches and
182 element definition. D: schematic of the aggregated morphological elements and their
183 connectivity.

184

3 MATERIALS AND METHODS

3.1 Macro-scale morphological model

3.1.1 Model concept

The model used to simulate the morphological evolution of the estuary is the macro-scale (scale-aggregated) numerical model ASMITA (Aggregated Scale Morphological Interaction between Tidal basin and Adjacent coast). This is an equilibrium-based model that was first proposed by Stive et al. (1998) for the study of estuary and inlet response to sea-level rise and extended to complex estuarine systems with more realistic forcing by various authors (Townend et al., 2016a,b). We used ASMITA version 1.5 (Townend, 2021), that is an extension of the model presented by Townend et al. (2016a). The most rudimentary estuary model has three elements to represent the channel, tidal flats and delta, and is forced by sea level rise (as in the model of Stive et al., 1998). As part of the more recent development of the model, additional types of elements and the ability to incorporate littoral drift have been added. These elements now provide for saltmarsh and storage (e.g., managed realignment sites), and a breakdown of the estuary mouth to include flood and ebb delta, and delta flats. In particular, the present model includes the implementation of an improved representation of drift on the open coast.

The modelling approach consists of a schematization of an estuary with its main morphological elements viewed at an aggregated scale. The main assumption is that, under constant hydrodynamic forcing, each element tends towards a morphological equilibrium which can be defined as a function of hydrodynamic forcing and basin properties. Each element is described in terms of its surface area, volume, and the horizontal and vertical rates of exchange. To introduce the main variables and parameters, a simplified equation for a single element model can be written as:

$$\frac{dV}{dt} = \frac{1}{c_b}\frac{w\delta C_E S}{\delta + wS}\left[\left(\frac{V_e(t)}{V(t)}\right)^n - 1\right] + SR \ , \quad (1)$$

where V is the element volume, V_e is the element equilibrium volume that depends on the tidal prism, and S is the element area (van Goor et al, 2003). For some features, V and V_e are water volumes (channels, saltmarshes, storages), for others they are sediment volumes (ebb delta) and for some they can be either (flood delta, flats, see Section 3.1.2).

The calibration parameters are c_b, the concentration of the bed that depends on the bed porosity, w, the vertical exchange coefficient, δ, the horizontal exchange coefficient and n, the transport coefficient. C_E is the equilibrium concentration of the system (usually taken as the open boundary value) and determines the morphological response time and so is generally used as the main calibration coefficient. Moreover, the model requires calibration parameters for the littoral and fluvial drift (q), and for the saltmarsh model (see Sections 3.1.4, and 3.1.5, respectively). Some parameters apply to the whole system (C_E), or to specific elements (n, w, c_b), whilst other parameters depend on the exchange between two elements (δ, or q). The main forcing, R, is given by the rate of sea level rise (in mm/year). A long-term variation in tidal range (e.g. lunar nodal tidal cycle, period of ~18.6 years) that affects the tidal prism, but not R, can also be considered in the model (Townend et al., 2007).

3.1.2 Geometric characterization

Each element is represented by an initial volume (V) and surface plan area (S). V can be a water or a sediment volume (Wang et al., 2008; Rossington et al., 2011). The channels are identified with a water volume. They are defined using the low water area and volume below this surface. The tidal flats (considered here as water volume elements) are defined as the area between high and low water and the volume below high water and over the flats (i.e., excluding the part of the tidal prism that is over the channel).

The saltmarsh element is defined by its plan area and the water volume over the saltmarsh. Sediment volumes are defined as the volume of sediment above an undisturbed coastal bed. For instance, the ebb delta can be represented by the sediment volume above the depth of closure, and its corresponding area. In addition, the cross-sectional area for the interface between elements is needed. For tidal flats, this is derived from the reach length and the mean tidal range, and for channels this is defined based on the cross-sectional area of the transect (vertical surface) between two adjacent elements.

3.1.3 Parameterization of the global equilibrium concentration, transport coefficient and vertical exchanges

The value of the global equilibrium concentration (C_E, in kg/m^3) is the concentration that would exist throughout the system when it is in equilibrium. Conceptually this should be the concentration of the background environment – in this case the open sea condition. However, this overlooks processes that can lead to higher concentrations within the estuary at equilibrium, such as tidal pumping (Scully and Friedrichs, 2007) and a mean concentration may be more representative. There is no rule to determine C_E, and its value is generally used to calibrate the morphological response time of the estuaries based on observations (Wang et al., 2008). Typical values used in previous studies range from 0.2-0.64 kg/m3 (Townend et al., 2016b).

The transport coefficient (n) is the concentration transport exponent and is akin to the power in a power-law sediment transport formula. On this basis, a value of around 3 is suitable when suspended sediment transport is dominant, whereas a value of 5 is more appropriate when bed load dominates, and these values should vary depending on the

types of sediment in the estuary. Note that positive values are used for water volume elements while negative values are used for sediment volume elements.

The vertical sediment exchanges (w, in m/s) refer to the rates of exchange between the bed and the water column and the same rate is applied for exchanges in either direction. It can be approximated to the sediment fall velocity, that depends on the sediment grain size and on the sediment density.

3.1.4 Parameterization of the horizontal sediment exchanges, littoral drift, and river discharge

The horizontal sediment exchange (δ, in m^3/s) depends on the cross-sectional area of the interface between adjacent elements and the tidal excursion distance which is estimated from peak tidal velocities across the interface. The latter can be estimated from flow modelling. Different relationships are used depending on whether the exchange occurs (1) between two channels, or between a channel and a delta, or between two delta elements, or (2) between the channel and an element that is tidal flat or saltmarsh (Townend, 2021). The following formulas are used:

$$\begin{cases} \delta = (\pi/T_p)\, u\, (HA/w), \text{ between two channels, or with deltas} \\ \delta = (\pi/T_p)^2\, (tr/2)\, (V/w), \text{ between channel and flats or saltmarshes} \end{cases}, \quad (2)$$

where T_p is the tidal period in seconds, u is the peak velocity obtained from numerical modelling, H is the hydraulic depth (we consider that $H=V/S$), A is the cross-sectional area of the interface between the elements, w is the vertical sediment exchange rate, and tr is the mean tidal range.

The littoral drift (sediment drift advection) is included in ASMITA in the same way as the river discharge (river flow advection). By considering the single element equation (1), where the contribution of sea level rise has been removed for the sake of simplicity,

the sediment flux entering (q_{in}) and exiting (q_{out}) a given element can be implemented as follows (Townend et al., 2016b):

$$\frac{dV}{dt} = \frac{1}{c_b}\frac{wC_E S}{\delta + wS}\left[(\delta + q_{out})\left(\frac{V_e(t)}{V(t)}\right)^n - (\delta + q_{in})\right] . \quad (3)$$

The drift is specified for each linkage as littoral drift (i.e. a volume of sediment per year – m^3/year). It can be estimated from a previous littoral dynamic study, based on observations of bathymetry evolution, sediment transport measurements, or hydro-sedimentary modelling. In keeping with the aggregated-scale of the model, the drift representation is simplified. The sediment fluxes entering and exiting the different littoral elements, as well as the whole estuarine system are difficult to estimate. Consequently, the flux rates should be calibrated and/or sensitivity analyses used to assess the how the fluxes contribute to model uncertainty. The advection through the model due to the river discharge is more straightforward (at least for a single channel system) because a mass balance must be maintained and the flux entering and exiting the channel elements is computed as a function of the river water flux, in m^3/s.

3.1.5 Salt-marsh parameterization

The implementation of the saltmarsh model in ASMITA was introduced by Knaapen et al. (2009) and based on the study of Morris et al. (2002) who derived a saltmarsh surface elevation evolution equation by considering the rate of sediment loading due to vegetation decomposition and the efficiency of the vegetation as a sediment trap. The volume change in the saltmarsh can be represented by the following equation that has been obtained from the single element equation (1), where the contribution of changes in sea level has been omitted (Townend et al., 2016b):

$$\frac{dV}{dt} = \frac{1}{c_b}\frac{w'\delta C_E S}{\delta + wS}\left[\left(\frac{V_e(t)}{V(t)}\right)^n - 1\right] - \sum_i \left(k_{b,i} B_i\right) V \quad . \tag{4}$$

In this equation w' is the modified fall velocity that reflects the additional dissipation of the kinetic energy due to the vegetation and the influence of trapping that depends on the fall velocity and the total biomass. The second right hand term represents the volume changes produced by the species (represented by the index *i*), where each species is represented by its biomass (B_i, in kg/m^2), and by a rate of productivity ($k_{b,i}$, in m^2/kg/year).

The biomass of each species depends on its geometrical characteristics and on the global equilibrium depth of the saltmarshes (*D*), that depends not only on the species characteristics but also on the rate of sea level rise and on the sediment concentration (Morris et al., 2002). The ASMITA graphical interface allows the user to apply the Morris et al., 2002 method to calibrate the saltmarsh species productivity ($k_{b,i}$), as a function of the maximum biomass ($B_{i,max}$), and the minimum, and the maximum depth ($D_{i,min}$, $D_{i,max}$) of each species, in order to obtain the desired marsh equilibrium depth, D. Assuming that the current saltmarsh system is in equilibrium, D can be seen as the mean depth of the salt-marsh platform with respect to a reference high water level. In this formulation, the depth is a surrogate for the hydroperiod of the saltmarsh.

3.2 Process-based hydrodynamic model

The Delft3D process-based model (Roelvink & Van Banning, 1995) including wave driver, shallow water equations and sediment transport, has been used in its hydrodynamic (fixed bed) depth-averaged (2DH) mode, to provide current velocities and sediment transport data along the estuary. We used the parameterization presented by Monge-Ganuzas et al. (2017), with a calibration based on data collected from current

meters and pressure sensors during 2015 campaigns with instruments deployed in subtidal and intertidal areas of the outer estuary. A double mesh is used for the wave model: a coarse regular mesh (resolution of 1 km) to propagate the waves from the Bilbao-Vizcaya wave buoy to the estuary and a finer curvilinear mesh (resolution of up to 10 m) to obtain the detailed wave patterns in the estuary inlet. A similar curvilinear mesh is used for the flow model to obtain the current velocities and the sediment transport. The model has been forced by mean wave conditions and the results used for the parameterization of the sediment exchanges in ASMITA, for spring tide conditions.

3.3 Data

3.3.1 Hydrodynamic forcing

The primary forcing condition is tidal, based on the tidal range and mean sea level, coupled with a rate of sea level change. The semi-diurnal tides are defined using mean tidal elevations and tidal constituents (M2 and S2) near the mouth of the estuary. Furthermore, the long-term variations in tidal amplitude due to the lunar nodal tidal cycle (period of ~18.6 years) are also included in the modelling. This information is obtained from the data of the Bilbao tidal gauges (Puertos del Estado, http://www.puertos.es, longitude: 3.05W, latitude: 43.35N, 1992-2021). These data are also used to characterize the mean sea levels needed to obtain the initial conditions of ASMITA (element volumes and surfaces, saltmarsh species properties).

The past, present, and future rates of sea level change considered here are obtained from borehole data analysis undertaken in the Oka estuary (García-Artola et al., 2015; 2018, hindcast data), from the current trends in sea level changes for the Bay of Biscay reported by Chust et al. (2022), and from the last projections of global mean sea level

352 presented in the Sixth Assessment Report of the Intergovernmental Panel on Climate
353 Change (AR6, IPCC, Fox-Kemper et al., 2021).
354
355 Wave data are used to obtain mean forcing conditions for the process-based modelling
356 as well as to investigate possible trends in the mean wave forcing to be considered for
357 future projections. We used the data of the Bilbao-Vizcaya wave buoy (Puertos del
358 Estado, http://www.puertos.es, longitude: 3.08W, latitude: 43.63N, 1990-2021) to
359 compute the mean wave regime. The mean wave regime has been considered as
360 constant for the forecast simulations in agreement with the results obtained by Chust et
361 al. (2022).
362
363 **3.3.2 Morphology and vegetation**
364 Bathymetric and topographic data have been used to compute the initial volume and
365 surface of the morphological elements, as well as to perform the process-based
366 modelling (Fig. 1B). Bathymetric data from deep water were needed to propagate the
367 waves from the Bilbao-Vizcaya wave buoy up to the estuary offshore boundary. Recent
368 high resolution topo-bathymetric data were needed for the hydro-sedimentary modelling
369 and to obtain the hypsometry of the estuary and of all the aggregated elements. For
370 these purposes, we used the 942 Spanish nautical charts for the offshore bathymetry
371 (Instituto Hidrográfico de la Marina), a 20 m resolution bathymetry from 100 m depth
372 to the coast (Basque Government, year 2009), a 1 m resolution topo-bathymetry for the
373 estuary mouth (MAGRAMA, Spanish Government, May 2015), and a 1 m resolution
374 topo-bathymetry for the lower and upper estuary (Basque Government, year 2009).
375

The saltmarsh species distribution is obtained from the data presented in the study of Chust et al. (2013) and Valle et al. (2015). The data have been used to identify the species properties needed to run the saltmarsh model. The information of the previous foraminiferal analysis from sediment cores taken in the Oka estuary has also been used in order to validate the results of the morphological simulations for both natural saltmarshes and for saltmarsh regeneration (Cearreta & Monge-Ganuzas, 2013; García-Artola et al., 2018).

3.4 Experimental procedure

3.4.1 Morphological model setup

The steps to define the elements and their respective properties were as follows:

i) Schematisation of morphological elements. Different approaches can be considered, depending on the dominant processes shaping the estuary (Rossington et al., 2011). We defined the morphological elements of the estuary/reach and its connections to represent an established conceptual behaviour model.

ii) Geometric characterisation. A GIS (Geographic Information System) analysis of the topo-bathymetry of the estuary was used. Polygons covering each estuary reach, with associated flat/delta and channel, were digitized and used to generate hypsometric curves, from which the geometric characteristics of the elements were defined.

iii) Parameterization of the global equilibrium concentration, transport coefficient and vertical exchanges. A first guess of the global equilibrium concentration was made based on previous ASMITA studies, and the transport coefficient and vertical sediment exchanges were determined based on the sediment characteristics of the estuary.

iv) Parameterization of the horizontal sediment exchanges, littoral drift, and river discharge. The horizontal sediment exchanges are a function of peak velocities and were obtained from a process-based numerical model. Littoral drifts were obtained from

401 sediment mass balance estimates, and river discharge was defined by the mean river
402 flow. ASMITA has the possibility of considering variable river flow conditions but this
403 was not included.
404 v) Salt-marsh parameterization. Data describing the saltmarsh species distribution, was
405 used to define the main species properties and the species productivity was treated as a
406 calibration parameter (Morris et al., 2002).
407

408 **3.4.2 Morphological model simulations**

409 Two types of simulation were undertaken, namely:
410 i) Hindcast simulations. Hindcast simulations were performed to calibrate and validate
411 the model. Hindcasting over a historical timescale was used to compare with changes
412 estimated from the available bathymetric data and foraminifera analysis (core).
413 Hindcasting over a geological timescale was used to compare with rates of infilling
414 estimated from the available borehole data. Calibration was undertaken following the
415 guidance on parameter setting provided by Wang et al., (2008). The hindcast
416 simulations were used to investigate:
417 - the response of the estuary to past sea level rise
418 - the effects of the lunar nodal tidal cycle in the morphological evolution of the estuary
419 - the morphological evolution of natural saltmarshes, drowned saltmarshes, and
420 saltmarshes in regeneration.
421 ii) Projections for a range of future climate scenarios. Simulations were made by forcing
422 the model with an exponential sea level rise based on IPCC scenarios and compared
423 with simulations of linear sea level rise.
424

4 MORPHOLOGICAL MODEL SETUP

4.1 Morphological element definitions

The Oka estuary has been divided into nine morphological elements (Fig. 1D) based on the conceptual models presented by Liria et al. (2009) and Monge-Ganuzas et al. (2015). They explore the mechanisms driving the sediment exchanges, both in the outer estuary, which is strongly influenced by waves, and between the outer estuary and the sheltered inner estuary, where the dynamics is dominated by tidal and riverine sediment transport. The outer estuary is formed by the estuary inlet, composed by the *ebb delta* (which includes the Mundaka sand bar), the *delta flats* (which includes the Laida beach), and the *delta channel* that makes the link to the inner estuary together with the *flood delta* (Fig. 1C,D). The inner estuary is divided into two reaches. The first reach (reach 1) is essentially sandy and formed by the *outer flats* and the *outer channel*. The second reach (reach 2) includes saltmarshes (*inner flat marshes*) connected to the *inner channel* through the *inner flats* that is composed of muddy sediment. In this study the part of the estuary at the upstream end of the artificial channel is not considered. It is composed of reclaimed areas, comprising saltmarshes, and a relict channel. The storage area next to reach 2 (indicated with the dashed line in Fig. 1C) is not included either. Including these elements would not change the results presented here, however, they are elements that can be added as potential adaptation options.

4.2 Geometric characterisation

The initial volume (V) and surface plan area (S) of the elements have been obtained from the hypsometry curves of different reaches of the estuary (Table 1). All the elements except the ebb delta are defined using water volumes. For all these elements, we used the mean low water level (MLW=0.95 m, with respect to the Bilbao port

450 datum) and the mean high water level (MHW=3.75 m) as reference. For the
451 saltmarshes, the reference high water level is the level of the mean high water springs
452 (MHWS=4.35 m). For the ebb delta. the undisturbed coastal bed level is at 10 m below
453 the low water level that corresponds approximately to the closure depth.
454

Table 1. Main properties of the morphological elements of the Oka estuary used as initial conditions for the ASMITA modelling: volume (V, m^3), surface (S, m^2), length (m), vertical exchange (w, m/s), transport coefficient (n), and bed concentration (c_b)

Morphological element	**Volume (10^6 m^3)**	**Surface (10^6 m^2)**	**Length (m)**	***w*** **(m/s)**	***n***	***c_b***
Delta channel	1.780	0.412	2850	0.02	5	0.385
Outer channel	0.465	0.136	900	0.02	5	0.385
Inner channel	0.920	0.246	4000	0.02	5	0.385
Outer flats	0.492	0.258	900	0.003	5	0.200
Inner flats	1.580	1.304	4000	0.003	5	0.200
Saltmarshes	1.234	1.151	4000	0.003	5	0.200
Ebb delta	3.504	0.405	600	0.02	-5	0.385
Flood delta	0.927	0.551	1500	0.02	5	0.385
Delta flats	0.891	0.466	750	0.02	5	0.385

4.3 Parameterization of the global equilibrium concentration, transport coefficient and vertical exchanges

Here, we used an intermediate value for the global equilibrium concentration of C_E=0.318 kg/m^3, based on previous ASMITA studies (Townend et al., 2016a), given that the dynamics of the estuary is governed by a mixed wave and tidal influence depending on the reach considered. This must be considered as a first guess value, as C_E is the final calibration parameter used to fit the model to the observed timescales of changes, once all of the other parameters have been set.

Concerning the transport coefficient (n), in keeping with the aggregated philosophy of the model, a representative value of +/- 5 was used for all elements (Table 1). As all elements, except the ebb delta, were defined as water volumes, these take a value of +5, whereas n=-5 was used for the ebb delta.

The vertical sediment exchanges (w) is approximated to the sediment fall velocity (Table 1). For the outer estuary and for the estuary channel, it was taken from the study of Al-Ragum et al. (2014), who obtained values of median grain size of d_{50}=0.1-0.3 mm in the outer estuary. For the inner estuary, we use typical values for muddy sediments that make up the flats and saltmarshes. A similar distinction is made for the bed concentration (c_b) which depends on the bed density. We use typical values for sandy beds for the inlet and main channels, and cohesive beds for the flats and saltmarshes.

4.4 Parameterization of the horizontal sediment exchanges, littoral drift, and river discharge

The parameterization of the horizontal sediment exchanges due to tidal dispersion (δ) was obtained from the results of the process-based modelling, which provided a representative value of the peak velocity (u, Equation 2) for each element, for typical wave and tide conditions. The results for mean wave conditions and for spring tides are presented in Fig. 2 (A and B). The waves were propagated from the vicinity of the Bilbao-Vizcaya wave buoy and the mean offshore conditions offshore are characterized by a significant wave height of Hs=1.6 m, a peak wave period of Tp=10 s, and a mean direction of 300º(W/NW). The maximum velocities are obtained in the delta channel (up to 1.8 m/s) and the minimum velocities are obtained in the upper estuary. The peak velocity u for each element has been obtained from the 95th percentile of the maximum current velocity magnitude obtained during a spring tide cycle (Fig. 2A), within the

494 element shape. The corresponding horizontal sediment exchange rates δ are indicated in
495 Fig. 2C.
496 The parameterization of the littoral drift (*q)* has been obtained from representative
497 values of sediment transport based on observation of the estuary mouth evolution
498 (Monge-Ganuzas et al., 2013; Gainza et al., 2019), but there is a large uncertainty in
499 quantifying both the exchanges between elements, and the sediment input and output to
500 the system. The main parameter that has been set is the exchange between the ebb-delta
501 and the delta flats that has been estimated to q~100.000 m^3/year (Fig. 2D). This
502 corresponds to the approximate volume of sediment mobilized during the yearly
503 onshore migration of the longshore bar and its eventual welding to the shore (Gainza et
504 al., 2019). Furthermore, we can state that the orders of magnitude of the exchanges
505 between the ebb-delta, the delta flats and the delta channel are similar. Finally, we
506 considered a small sediment input, and an even smaller sediment output consistent with
507 the observed transgression of the estuarine system. The values of the sediment transport
508 used were best estimates based on the data available and could be further calibrated
509 using more detailed observations of the inlet. In the present study, because the whole
510 estuary is assumed to be in equilibrium (at the reference time), and we consider constant
511 wave forcing and sediment input/output, changes in these parameters do not affect the
512 results. Further investigation would be needed to calibrate the fluxes for time varying
513 conditions, due, for example, to climatic variations in wave conditions, but this was
514 beyond the scope of the present study.
515 An option to determine the sediment transport exchange coefficient is to use a process-
516 based model. For this study, the process model was run using the default sediment
517 transport formulations, and results of mean sediment transport, resolved in and out of
518 the estuary, were obtained for the same spring tidal cycle and for the same mean wave

519 conditions as presented above (Fig. 2B). This provided a characteristic estimate and
520 more realistic results could be obtained from multiple simulations and statistical
521 techniques to propagate the historic wave series. However, the results indicate a
522 maximum offshore transport in the delta channel, and a maximum onshore transport at
523 the interface ebb-delta / delta flats, with the same order of magnitude (q~100.000
524 m^3/year, was obtained by integrating the mean sediment transport in m^3/m/year over the
525 interface cross-section).
526 Finally, the river discharge was introduced in all the channel elements and was assumed
527 to be constant, and in balance in all the elements. The mean river flow was obtained
528 from the study of Peraza-Castro et al. (2018), and is q_{river} = 0.63 m^3/s.
529

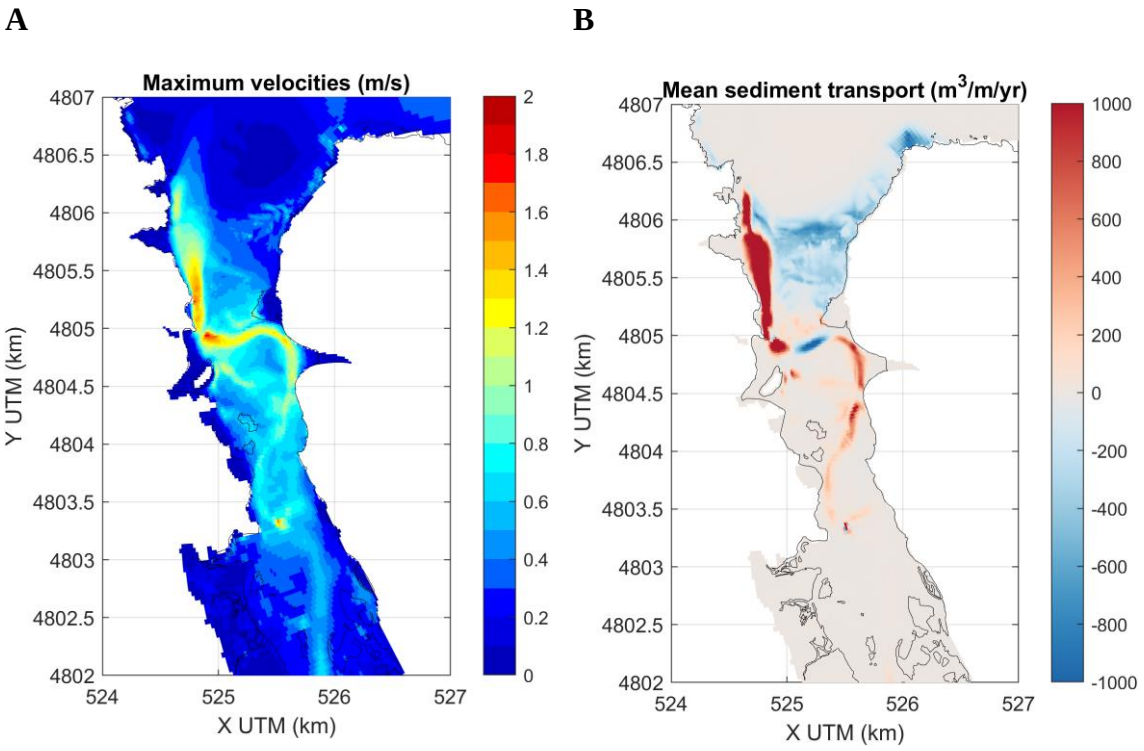

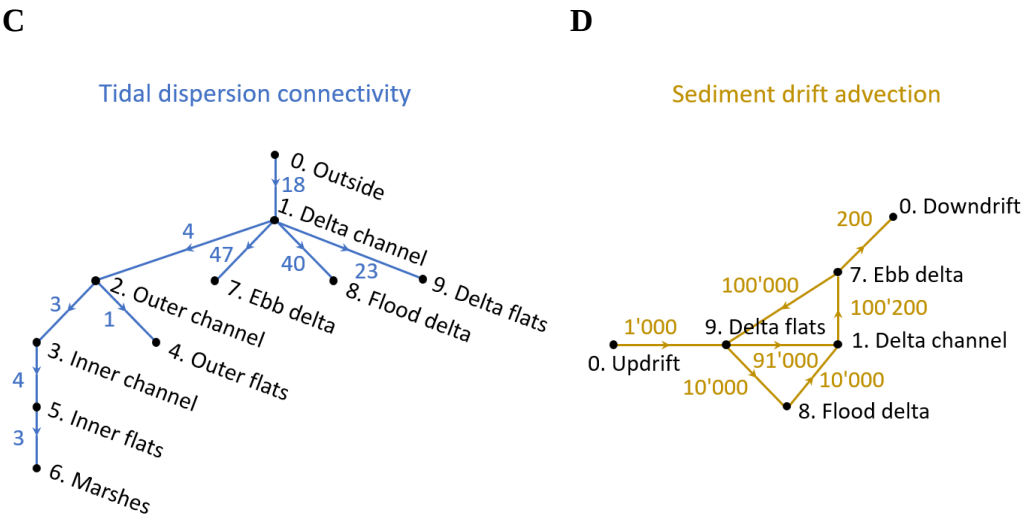

530 Fig. 2. Results of the simulations of the process-based model and horizontal sediment
531 exchanges. A: maximum current velocity magnitude obtained during a spring tide tidal
532 cycle (in m/s) for mean wave conditions. B: mean sediment transport obtained during a
533 spring tide tidal cycle (in m^3/m/year) for mean wave conditions, positive values (red)
534 indicate offshore transport, negative values (blue) indicate onshore transport. C: tidal
535 dispersion connectivity and horizontal sediment exchange coefficients (δ, in m^3/s). D:
536 sediment drift advection (littoral drift) and sediment transport coefficients (q, in
537 m^3/year).

538 **4.5 Salt-marsh parameterization**

539 The vertical distribution of three saltmarsh species were included in the model (Fig. 3):
540 (1) a pioneering saltmarsh species composed by *Spartina maritima*, (2) a mid saltmarsh
541 species composed by *Halimione portulacoide* and *Puccinellia maritima*, and (3) a high
542 saltmarsh species dominated by *Juncus maritimus*, as well as the distribution of *Zostera*
543 *noltei* seagrass observed on the intertidal flats. These results allowed us to obtain the
544 minimum and maximum depth ($D_{i,min}$ and $D_{i,max}$) of the different species that are used as
545 input parameter in ASMITA (Table 2). They are defined based on the 5th and 95th
546 percentile of the vertical distribution, with respect to the level of the mean high water
547 springs (MHWS). The maximum biomass values ($B_{i,max}$, Table 2) were obtained from

548 the study of Benito and Onaindia (1991) and used to calibrate the species productivity
549 (k_b) in order to obtain an initial equilibrium depth of the saltmarsh D=0.6 m. It is
550 defined as the depth of the main saltmarsh platform, that is located approximately at the
551 level of the mean high water. The adjustment of the rates of productivity (Table 2) was
552 obtained following the method of Morris et al. (2002) using the ASMITA graphical
553 interface.

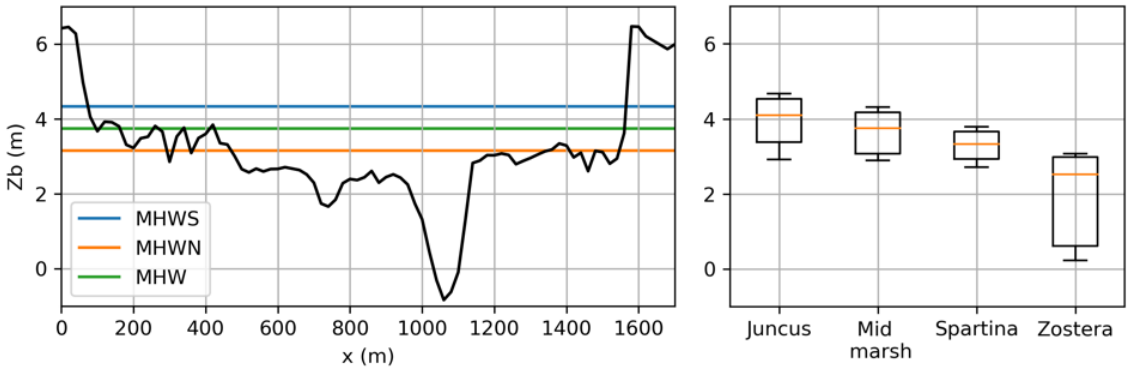

554

555 Fig. 3. Saltmarsh species distribution in the Oka estuary. Left: example of a topo-
556 bathymetric section in the Busturia area (Y_{UTM}= 4,802,500 m) with the indication of the
557 levels of the mean high water springs (MHWS, blue line), the mean high water (MHW,
558 green line) and the mean high water neaps (MHWN, orange line). Right: species
559 distribution along the vertical range: high saltmarsh (*Juncus maritimus*), mid saltmarsh
560 (*Halimione portulacoides*, *Puccinellia maritima*), pioneering saltmarsh (*Spartina*
561 *maritima*) and *Zostera noltei* meadows. The boxes indicate the 5th and 95th percentile of
562 the vertical distribution, the black bar the minimum and maximum height and the
563 orange bar the median height.

564

565

Table 2. Results of the saltmarsh model calibration. Properties of the main species used as input in the ASMITA model. For each species, minimum and maximum depth of the saltmarsh with respect to the level of the mean high water springs ($D_{i,min}$ and $D_{i,max}$), maximum biomass ($B_{i,max}$), and rate of productivity ($k_{b,i}$).

Species	$D_{i,min}$ **(m)**	$D_{i,max}$ **(m)**	$B_{i,max}$ **(kg/m^2)**	$k_{b,i}$ **(m^2/kg/year)**
Spartina	0.78	1.31	0.5	0.15
Halimione - Puccinellia	0.32	0.96	2	0.015
Juncus	-0.12	0.59	2	0.015

5 MORPHOLOGICAL MODEL SIMULATIONS

5.1 Response of the estuary to past sea level rise

The results of detailed borehole analysis have allowed chronologies of relative sea level rise to be prepared for several sites on the Atlantic coast (Garcia-Artola et al, 2018), one of which is the Oka. These equate to timelines of the sedimentation that have taken place over the last 10-12,000 years, and they suggest a rate of relative sea level rise over the last 1-2,000 years of between 0.3 and 0.7 mm/year. In addition, the analysis of sediment cores, taken from the saltmarsh in the Oka, has much greater resolution over the last 2-300 years and provides evidence of a more recent acceleration in the rate of sea level rise (Garcia-Artola et al, 2015). Given the confined nature of the antecedent river valley, it is reasonable to assume that the plan area has remained approximately constant at about $5x10^6$ m^2. With the projected sea level rise, this suggests that between 1,500 and 3,500 m^3/year of sediment were imported to maintain the estuary system relative to the rising tidal frame. Simulating the last 2000 years in the ASMITA model,

gives comparable rates of infilling namely 1,550 and 3,560 m^3/year respectively. Using a slightly higher rate of 1 mm/year, the model infills at a rate of 5,070 m^3/year, with no evidence that any of the elements are unable to keep pace, suggesting that the adaptation capacity of the system is higher than demanded by past rates of sea level rise.

The next set of simulations considers a linear sea level rise based on a rate of R=1.7 mm/year representative of observations for the last century (García-Artola et al., 2015). The astronomical tide parameters considered for these simulations have been obtained from the harmonic analysis of the Bilbao tidal gauge and are the mean tidal range (tr=2.8 m), and the M2 and S2 constituents (M2=1.31 m, S2=0.45 m). Results are given for the time period 2000-2100 and have to be considered as a baseline study to be compared to projections based on climatic studies (see Section 5.4) and as a representation of the morphological changes observed in the past. It should be reminded that current sea level rises observed in the Bay of Biscay are higher (R=1.5-3.5 mm/year, Chust et al., 2022), as well as the rates obtained from projections (R=5-10 mm/year in the Bay of Biscay, Chust et al., 2010), and even higher rates are obtained from the last IPCC global results (Fox-Kemper et al., 2021, see Section 5.4).

For this linear sea level rise, the different morphological elements of the estuary have the same behaviour (Fig. 4). The fixed volume of all the elements, except of the ebb delta, decreases in time. It is defined as the volume below a fixed initial surface (the initial water level), so that it ignores any changes in the water level and it therefore represents the sedimentation/erosion volume occurring in the elements. Because these elements are defined using water volumes, a decrease of the fixed volume means that there is sediment deposition over the element. Similarly, an increase of the fixed volume

of the ebb delta (the element defined with a sediment volume) implies that there is also sediment deposition over the delta. In contrast, the moving volume includes both the morphological changes, and the water volume changes, and is equivalent to the total change in the water/sediment volume. For all the elements, the moving volume is approximately constant. This means that all the elements keep pace with the sea level rise: there is sedimentation in all the elements, at the same rate as sea level rise. This result agrees with the hypothesis outlined in earlier studies (Cearreta & Monge-Ganuzas, 2013; García-Artola et al., 2018). It should be noticed that one implication of this result is that the tidal prism of the estuary is constant for these conditions of linear sea level rise.

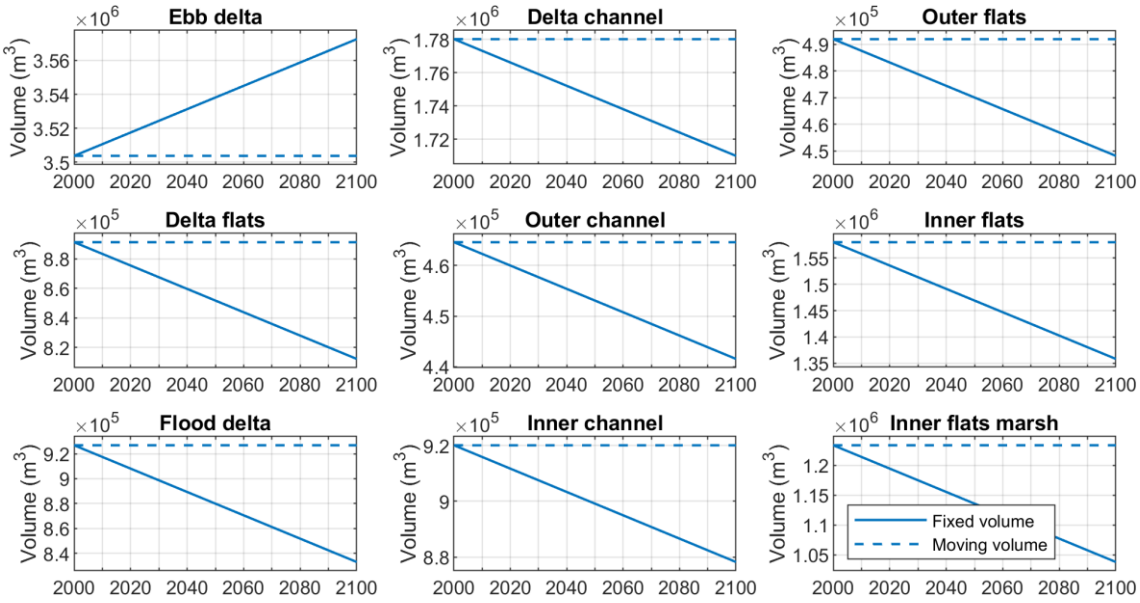

Fig. 4. Response of the Oka estuary to a linear sea level rise. Time evolution of the fixed volume (solid line) and of the moving volume (dashed line) for the different morphological elements represented in ASMITA. Notes: (i) scale on y-axis varies; (ii) the dashed line are horizontal - this means that the estuary keeps pace with the sea level rise and that a similar sedimentation is obtained in all elements; and (iii) an increase in

sediment volume (ebb delta) is equivalent to a decrease in water volume (the other elements).

5.2 Effects of the lunar nodal tidal cycle in the morphological evolution of the estuary

The results obtained here are highly simplified. This is inherent in the concept of the macro-scale ASMITA model, plus, we consider a constant input of sediment from the shoreface and from the rivers, a constant forcing (a linear sea level rise), and a constant parameterization (current velocities and sediment transport based on mean conditions), the objective of these simulations being to understand how the estuary will evolve in idealized conditions. We therefore focus on long term changes observed during the last centuries. Over shorter time scales, and when trying to relate the results to historic changes, shorter-term perturbations, such as the lunar nodal cycle can also be important (Townend et al, 2007; Wang and Townend, 2012). An analysis of the time series of the yearly mean tidal range obtained from the 40 years of sea level data of the Bilbao tidal gauge shows a clear oscillation with a period of 18.6 years corresponding to the lunar nodal tidal cycle (Fig. 5). A harmonic analysis determined the amplitude of the nodal oscillation to be 9 cm.

By including the effect of the nodal tidal cycle, i.e., by considering a varying tidal range at the same time as the mean sea level increases linearly, the simulated bed perturbation (h) does not increase linearly (i.e., as in the previous simulation, Fig. 4, or blue lines in Fig. 5). By looking at the saltmarsh element (Fig. 5), the bed perturbation oscillates around a mean position that corresponds to the case without nodal tide (linear increase). The oscillation has the period of the nodal tide (18.6 years), but it has a positive phase

shift with respect to the tidal range signal (~+5 years), implying that the highest yearly mean tidal range observed in the last two decades that occurred in 2015 caused a maximum deposition in the saltmarsh in 2020. Consequently, the model predicts a local maximum deposition in the saltmarsh every 18.6 years due to the nodal tidal cycle. Therefore, the effect of the nodal tide causes an increasing and decreasing rate of bed deposition (dh/dt) relative to the constant rate of 1.7 mm/year obtained in the previous simulation (without nodal tide). In particular, the rates vary between -3.3 mm/year (this means that, at these times, the depth over the saltmarsh increases more than the sea level rises) and 5.4 mm/year (maximum deposition rate, the sediment deposition is faster than the sea level rise), implying that there is a deviation of between -5 mm/year and +3.7 mm/year in the saltmarsh deposition rates due to the nodal tidal cycle. These maximum and minimum deposition rates are approximatively in phase with the maximum and minimum values of the yearly mean tidal range, meaning that the maximum sediment deposition rates obtained in the saltmarsh occurred in 2015, and this rate will occur every 18.6 years (when considering a linear sea level rise).

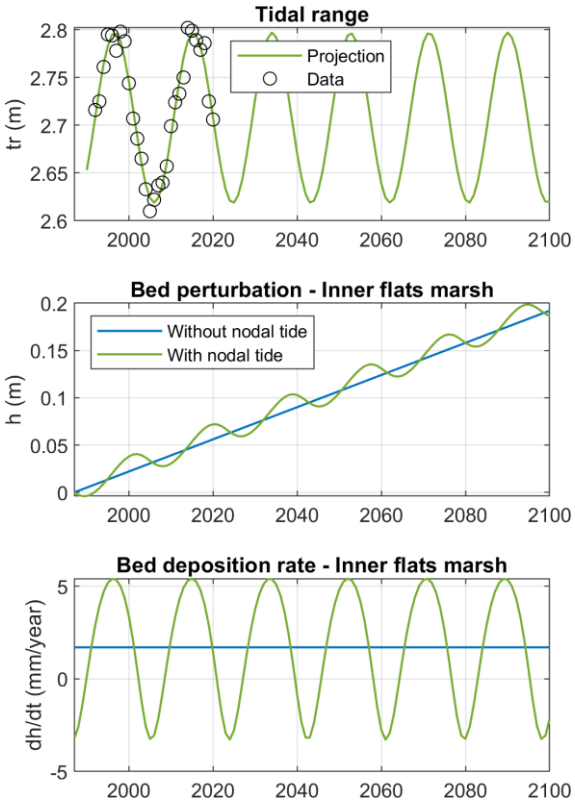

671

672 Fig. 5. Effects of the lunar nodal tidal cycle in the morphological evolution of the Oka
673 estuary. Top: yearly mean tidal range obtained from the sea level data of the Bilbao tidal
674 gauge (1992-2021, black circles), and harmonic reconstruction of the tidal range until
675 2100 (green line). Middle: simulated time evolution of the bed perturbation (h, in m)
676 over the saltmarsh element by including (green line) and excluding (blue line) the nodal
677 tidal cycle. Bottom: simulated time evolution of the rate of bed deposition (dh/dt, in
678 mm/year) by including (green line) and excluding (blue line) the nodal tidal cycle.

679

680 **5.3 Morphological evolution of natural saltmarshes, drowned saltmarshes, and**
681 **saltmarshes in regeneration.**

682 The saltmarsh model takes due account of the biological contribution to sedimentation
683 and the effect of sedimentation on biology. In particular, the saltmarshes contribute to
684 the sedimentation of the estuary, as, if multiple species can coexist, the increasing sea
685 level will be associated to an increasing biomass and therefore to sediment trapping and

biological production. To quantify this effect, new simulations were performed by comparing results with and without the bioproduction of saltmarshes (Fig. 6A). This is equivalent to a hypothetic case of drowned saltmarshes, where saltmarshes would behave as tidal flats without vegetation. As expected, the results indicate less deposition over the drowned saltmarshes and show the importance of the saltmarsh bioproduction for the sedimentation of the estuary. In particular, the sedimentation rate decreases from 1.7 mm/year when bioproduction is included (default model parameterization, case of natural saltmarsh) to almost 1 mm/year when the bioproduction is omitted (case of drowned saltmarsh). In this latter case, the system does not keep pace with the linear rate sea level rise.

Previous studies have shown that the sedimentation in saltmarsh that are in the process of regeneration following a period of enclosure (i.e., saltmarshes previously reclaimed that have been re-opened), can be much faster than in natural saltmarshes (Cearreta et al., 2002; Cearreta et al., 2013; Sainz de Murieta, 2016; García-Artola et al., 2015). The effect of saltmarsh re-opening was investigated by perturbing the saltmarsh from its equilibrium depth. To do this, the disequilibrium depth was estimated by considering the loss of accretion over the period when the saltmarsh was inactive due to enclosure, relative to a saltmarsh that was open and able to accrete. The difference defined an excess-depth which was used to estimate the disequilibrium volume that defines the initial condition when the saltmarsh is re-opened.

The simulations of a saltmarsh re-opening in the year 2000 considered an occupation time of 300 years, with a disequilibrium depth of 51 cm (sedimentation rate of 1.7 mm/year), are shown in Fig. 6B. A higher sedimentation is obtained in the case of the

711 regenerating saltmarsh than in the natural saltmarsh case. In agreement with previous
712 studies, the sedimentation rate is stronger during the first years after the opening. The
713 maximum deposition rate is 20 mm/year just after the opening and is more than one
714 order of magnitude larger than for the natural saltmarsh during the first decade.
715 Although this case is hypothetical and highly simplified compared to a real opening, the
716 order of magnitude of the deposition rates obtained agrees with the observation based
717 on foraminifera studies. They obtain rates of 16 mm/year during the first 10 years after
718 the opening (Cearreta et al., 2013), and rates even higher are obtained in some locations
719 (García-Artola, 2013).
720
721
722
723
724

A. Effect of saltmarsh bioproduction **B.** Effect of saltmarsh opening

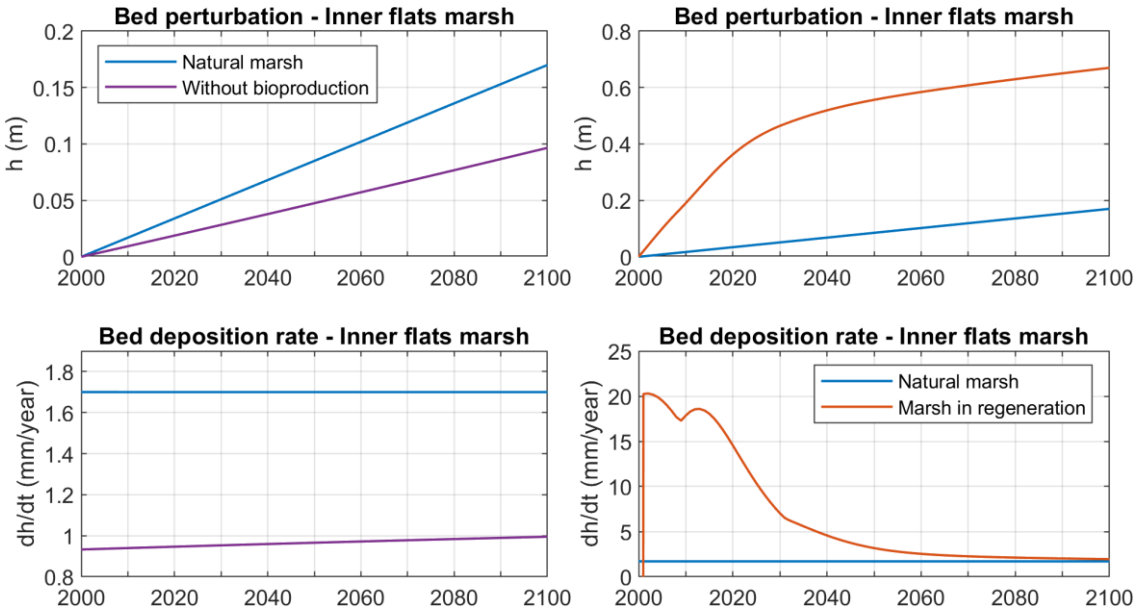

Fig. 6. Morphological evolution of natural saltmarshes, drowned saltmarshes, and saltmarshes in regeneration. Simulated time evolution of the bed perturbation (h, in m, top plots) and of the bed deposition rate (dh/dt, in mm/year, bottom plots). A: Simulations including (blue line, natural saltmarsh) and excluding (purple line, drowned saltmarsh) the saltmarsh bioproduction. B: Simulations for a natural saltmarsh (blue line) and a saltmarsh in regeneration (saltmarsh opening, orange line, opening date: 2000).

5.4 Response of the estuary to projected sea level rise

The previous results indicate that the estuary keeps pace with a linear rate of sea level rise of R=1.7 mm/year, given that sediment deposition occurs in all the morphological elements at a similar rate. The response of the estuary to an exponentially increasing rate of sea level rise was investigated because this potentially more closely represents the current rate of change and future projections. The forcing considered is the

739 exponentially increasing sea level and for the sake of simplicity, only the case of the
740 natural saltmarsh is shown, disregarding the effect of the nodal tidal oscillations that
741 would produce a periodic variability to the results without changing the conclusions.
742
743 The first sea level conditions have been obtained from the exponential fit of the relative
744 sea level data obtained from the foraminifera study of García-Artola et al. (2015) (Fig.
745 7A, the data are indicated with the black circles, and the exponential fit is the black
746 line). The other sea level forcing conditions are obtained from the global mean values
747 published in the AR6 IPCC report (Fox-Kemper et al., 2021). Each exponential sea
748 level projection used in the model was obtained from the results of projected rates of sea
749 level for 2050 and 2090 (in mm/year), and of the value of the projected sea level for
750 2100 (in m). We considered two SSP scenarios as defined in the latest IPCC report, the
751 medium-low emission scenario SSP2-4.5, and the high emission scenario SSP5-8.5.
752 Median values and likely (17^{th}-83^{rd} percentile) range values have been used to obtain
753 the median exponential sea level rise (thick colour lines), and the confidence interval
754 (shaded colour bands, Fig. 7A,B).
755
756 The first result obtained from the exponential fitting of the relative sea level values is
757 the similarity between the exponential fit of the foraminifera data with the IPCC
758 projection values, precisely with the median values of the SSP5-8.5 scenario (Fig. 7A).
759 In both cases, the predicted sea level rise for the year 2100 is between 0.7 m and 0.8 m,
760 relative to year 2000 (in the IPCC study, results are given relative to a baseline of 1995-
761 2014). In the worst of the scenarios considered in the present study, the maximum
762 relative sea level is about 1 m (83^{rd} percentile of the SSP5-8.5 scenario), and, in the best
763 scenario, the relative sea level obtained in 2100 is something less than 0.5 m (13^{rd}

764 percentile of the SSP2-4.5 scenario), that is almost three times the relative sea level
765 considered in the previous simulations for 2100 with the linear sea level rise of 1.7
766 mm/year.
767
768 Simulations performed for the foraminifera exponential sea level curve as well as for
769 the exponential sea levels of the IPCC report are shown for saltmarsh mobile volume
770 change in Fig. 7B. The results indicate that for all the exponential sea level rises
771 considered, the estuary does not keep pace with sea level rise, contrary to what
772 happened when using a linear rate of sea level rise. When the morphological elements
773 keep pace with sea level rise, the mobile water volume is constant (see for instance the
774 case of linear sea level rise in Fig. 4), so in this case there is no volume change (0%)
775 during the evolution. With the exponential sea level rise, the water volume increases
776 over the saltmarsh. In 2100, the water volume will increase by 2% (1%-3%, likely
777 range) in the medium-low emission scenario (SSP2-4.5), and by 6% (4%-12%, likely
778 range) in the high emission scenario (SSP5-8.5). These increases mean that the
779 sediment will deposit at a slower rate than the sea level rises in the saltmarshes. In other
780 words, the saltmarsh depth will increase (one of the hypotheses of the model is that the
781 water volume over the saltmarsh and the saltmarsh depth are proportional), that implies
782 that the hydroperiod will increase with the exponential sea level rise. Therefore, this 1%
783 to 12% increase of the saltmarsh depth predicted for the year 2100 may have
784 implications for the survival of individual saltmarsh species, and on the future extent of
785 the saltmarshes. Concurrently, the increase of the hydroperiod might provide new
786 suitable habitat to *Zostera noltei* seagrass meadows, since this species, contrary to
787 saltmarshes, is not affected by submersion, being able to survive if submerged
788 permanently.

A similar result is obtained for the other morphological elements of the estuary except for the ebb delta (Fig. 7C). The channel elements, the tidal flats, and the flood delta do not keep pace with the exponential sea level rise as the water volume above these elements increases in time. The ebb delta behaves differently: the sediment deposition is faster than the sea level rise. This can be seen in Fig. 7C where the thickness of the ebb delta strip decreases in time (dark blue strip). The displayed quantity is an adjusted water volume over the ebb delta. The ebb delta is therefore the only element where sediment deposits faster than sea level rises, but this is remains insufficient to compensate for the sediment deficit in the other elements (the cumulative water volume increases).

A

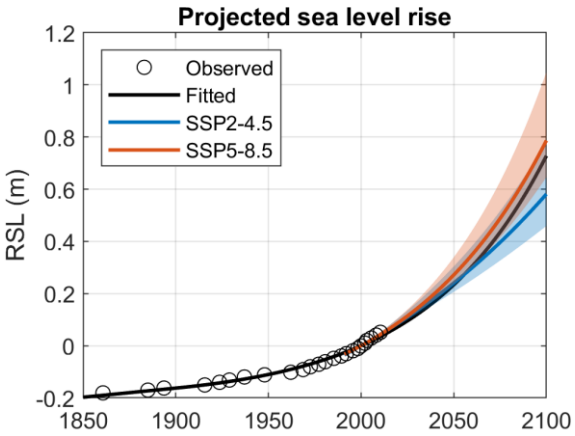

B

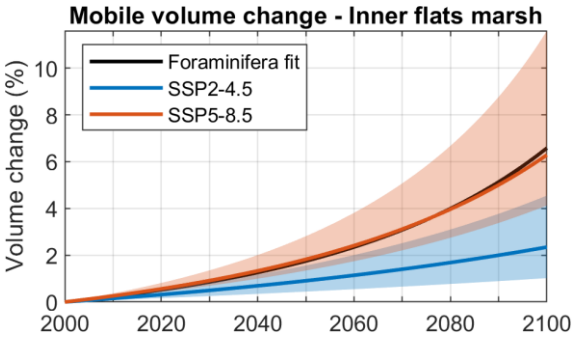

C

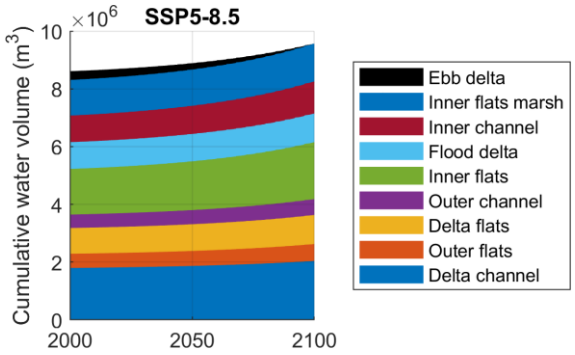

808

809

810

811

812

Fig. 7. Response of the estuary to the projected sea level rise. A: relative sea level (RSL, in m), the black circles indicate the data obtained from the foraminifera study of García-Artola et al. (2015), the black line is the exponential fit, the coloured lines are the exponential relative sea level increase based on the global IPCC projections (Fox-Kemper et al., 2021): scenarios SSP2-4.5 (orange line) and SSP5-8.5 (blue line). The lighter colour bands represent the 17^{th}-83^{rd} percentile range. B: time evolution of the increasing water volume over the saltmarsh (as a % of the initial water volume). C: time evolution of the cumulative water volume (in m^3) over the estuary, the coloured strips indicate the change in water volume of each element over time.

6 MODELLING LIMITATIONS AND FURTHER RESEARCH FOR THE DESIGN OF ADAPTATION MEASURES

6.1 Modelling limitations

The model simulations exhibit a general qualitative agreement with the past observations at an historical time scale. The model validation could be improved by studying the effect of past human interventions in detail. Here, we studied a case of saltmarsh opening, as a hypothetical schematization, where the entire saltmarsh area was reclaimed and then released. A more detailed analysis could be performed by dividing the saltmarsh area into several saltmarshes (also including the upstream saltmarsh), and endeavouring to hindcast a realistic opening chronology. Such an exercise might also include the effect of other past interventions, such as the land reclamation and saltmarsh draining. This analysis could also be extended to the geological time scale (Holocene time scale), similar to the work of Townend et al., 2007, using detailed borehole reconstruction to identify the pre-Holocene surface and the rate of infilling over the Holocene, as for example undertaken for the Humber

838 estuary (Rees, 2006). The simple estimates made as part of the model validation
839 (Section 5.1) show that for the recent Holocene (last 2000 years) during which the sea
840 level rise has been relatively benign, with a rate estimated at between 03 and 0.7
841 mm/year (Garcia-Artola et al, 2018), the estuary would keep pace with sea level rise
842 (assuming no reduction of sediment input in the system).
843
844 The present study could be improved by including more realistic (varying) forcing
845 conditions and changes in sediment input to the system; observed or in the future. A
846 constant wave forcing has been considered for hindcasting and forecasting in agreement
847 with climate studies that did not find significant trends in the mean wave regimes based
848 on wave buoy data (Chust et al., 2022), or on projections (Camus et al., 2017), but
849 including intra-year wave variability would merit further investigation. Moreover, in the
850 present study, the sediment input from the shoreface and adjacent beaches, and from the
851 rivers was assumed to be constant. At the time-scale of our analysis (order of 100
852 years), and when comparing the simulation to past events, these assumptions seem
853 reasonable, as the accretion rates observed in the saltmarshes have been correctly
854 reproduced. However, a more detailed sediment mass balance study (Peraza-Castro et
855 al., 2018; Amos et al., 2020), coupled with an accurate monitoring programme in
856 different parts of the estuary (French & Burningham, 2003; Liria et al., 2021) would
857 enable more detailed validation of model performance and may provide further insight.
858 At the same time, the sensitivity of the model simulations to changes in riverine and
859 marine sediment input need to be tested. The quantity of fine sediments contributed by
860 the rivers is relatively small and future variations in catchment run-off, and hence
861 supply, is unlikely to have any significant impact. In contrast, the marine supply has
862 been significant throughout the Holocene but future availability of sandy sediments is

more uncertain and any decline would have a significant impact on the future evolution of the Oka.

6.2 Further research needs

Human impacts increase the fixity of the estuary margins, also known as coastal squeeze (Dennis et al., 2000; Pontee, 2017). This has an impact on the results presented here. In particular, one of the assumptions of the present modelling is that the surface area of the elements is constant during the morphological evolution. This means that the estuary, with a well-documented history of marine transgression (Cearreta & Monge-Ganuzas, 2013; García-Artola et al., 2018), is assumed to infill and the elements would migrate landward keeping a similar surface area. However, the extent and rate of transgression are likely to vary, implying changes in the extent of tidal flat and saltmarsh surface in response to changes in the accommodation space of the estuary. The transgression of the estuary as function of the accommodation space, obtained from the shape of the pre-Holocene valley and equilibrium estuary form has been explored theoretically by Townend et al. (2021). Such response is predicted on the estuary being able to translate inwards within the valley landscape. This is however constrained by the presence of walls. The results presented in the present study can be considered as an optimistic situation where the volume of saltmarsh is not affected by a possible reduction of the saltmarsh area. Further research is needed to include the effect of coastal squeeze in the morphological evolution of the estuary.

Another aspect to consider for future projections is the biological implications of the results presented here. The increasing volume of water over the saltmarsh is equivalent to an increase of the hydroperiod, and this can affect the survival of the species and

have an impact on both saltmarsh development and accretion rates. On the other hand, modelled morphological changes and their consequences (such as the increase of the hydroperiod in saltmarsh areas) might provide new areas for *Zostera noltei* seagrass meadows in those areas where saltmarshes are currently present. However, other factors such as changes in the mean or extreme temperatures may affect the saltmarsh and seagrass species. Modelling their distribution and projecting it under future climate changes scenarios, which consider the modelled morphological changes, will help understanding future status of these ecosystems and suggesting adaptation measures to ensure their conservation.

6.3 Design of adaptation measures

Despite the simplifications inherent in the model, and the simplifications made in the discretization of the estuary and in the forcing conditions, the tools presented are able to provide information and insights that can be used to improve flood risk assessment studies and to design adaptation measures to climate change. First, the volume changes of each element of the estuary can be projected at a given date. This could be used to relax the rigid bed approximation typically made in flooding projections (del Campo et al., 2021). On the other hand, the simulations of saltmarsh opening have shown sedimentation rates in agreement with observations, enabling specific adaption options to now be examined.

The model is also able to investigate the effect of dredging/dumping interventions, that can be also studied as possible measures of adaptation. Experiments have been performed to reproduce the effect of past interventions. It was found that, in all the cases, the estuary system returned to its previous equilibrium state (the one without

intervention), but the response times of such interventions were larger than the observed times, as the geometric details of the interventions were substantially smaller than the model elements used in the schematization of the estuary. In addition, the numerical time steps of the model are of the order of months, which is similar to the time-scale of the response time that is being represented. For these reasons, a more detailed schematization, or a higher-resolution process-based modelling study is required to anticipate the behaviour of the estuary after such interventions, like the work of Monge-Ganuzas et al. (2017) and of Gainza et al. (2019), and should be used to complement a long-term equilibrium study.

7 SUMMARY AND CONCLUSIONS

The morphological response of the Oka estuary to climate change has been investigated by means of the behaviour-oriented aggregated-scale numerical model ASMITA. The model simulates the morphological interactions between different elements of the estuary and the adjacent coast and indicates their volumetric evolution. The outer and inner estuary were discretized into nine morphological elements. The outer estuary, where the mouth is strongly influenced by the effect of waves, comprised the ebb delta, the delta flats, the flood delta, and the delta channel. The inner estuary was divided into two reaches. The first reach was defined as essentially sandy and formed by the outer flats and the outer channel. The second reach included the saltmarshes connected to the inner channel through the inner flats composed of muddy sediments.

The model was parameterized based on previous sedimentary studies of the Oka estuary and previous studies using ASMITA. Some model parameters depend on the whole system, or on a specific element, other parameters depend on the sedimentary exchanges between two elements. The horizontal sediment exchange rates due to tidal dispersion

938 over the full estuary and the sediment transport fluxes due to sediment drift advection
939 over the estuary mouth have been estimated based on results of the hydro-sedimentary
940 process-based numerical model Delft3D that has been run for mean wave conditions
941 during spring tides. The saltmarsh model that includes the influence of sediment
942 trapping, the sedimentation due to biological production, and the competition between
943 saltmarsh species, has been parameterized based on data of species distribution.
944
945 By forcing the model with a linear rate sea level rise of 1.7 mm/year, a rate that is
946 consistent with the representative rate for the last century obtained from previous
947 foraminifera analysis, the estuary keeps pace with sea level rise, in agreement with
948 observations. An 18.6-year periodic variability of between -5 mm/year and +3.7
949 mm/year was identified over the saltmarshes due to the effect of the nodal tide, with the
950 last maximum in deposition occurring in 2020. The effect of the opening of a saltmarsh,
951 that was drained at the beginning of the 18^{th} century, has been investigated using a
952 simplified schematization. The modelling results showed strong sedimentation rates of
953 up to 20 mm/year, in general agreement with the rates obtained from previous
954 foraminifera analysis.
955
956 To predict the future response of the estuary, simulations with an exponential sea level
957 rise were obtained from the exponential fitting of relative sea level data from
958 foraminiferal analysis, and from the last IPCC projections for the medium-low emission
959 scenario SSP2-4.5 and for the high emission scenario SSP5-8.5. We see that the estuary
960 fails to keep pace with sea level rise in any of the scenarios considered. In particular, the
961 sediment deposits at a slower rate than the rate of sea level rise in the saltmarshes,

resulting in an increase in hydroperiod, that could have a negative impact on species survival.

Despite the simplifications inherent in the model, and the simplifications made in the discretization of the estuary and in the forcing conditions, the tools presented are able to provide information and insights that can be used to improve flood risk assessment studies and to design adaptation measures to climate change. Using this aggregated model in conjunction with a more detailed process model, served to reduce the uncertainty in model parameterization and supplement understanding of the important short-term processes that influence longer-term morphological evolution. As only volumetric changes and information on the equilibrium of the estuary are given by ASMITA, the higher-resolution process-based model again acts as a powerful adjunct, enabling potential changes in the more detailed hydro-sedimentary processes to be investigated for future epochs, or in response to specific possible interventions or adaptation measures.

ACKNOWLEDGEMENTS

This study is part of the Okaklima project sponsored by Ihobe (Basque Government) through the Klimatek 20-21 initiative. Roland Garnier acknowledges funding from the Provincial Council of Gipuzkoa through the Fellows Gipuzkoa Programme (Ref: 2020-FELL-000007-01). Part of this work is supported by the Urban Klima 2050 project from the EU LIFE programme (Ref: LIFE 18 IPC 000001) and from the MARLIT project from the EU Interreg POCTEFA programme (Ref: Va EFA344/19). This research responds to the objectives of the Kostarisk cross-border laboratory and of the EUSKOOS Basque Operational Oceanography System (https://www.euskoos.eus/). The

wave data from the Bilbao-Vizcaya buoy and the sea level data from the Bilbao tidal gauge have been provided by Puertos del Estado. An open source Matlab version of the ASMITA model is available at www.coastalsea.uk. This paper is contribution nº1129 from AZTI, Marine Research, Basque Research and Technology Alliance (BRTA).

REFERENCES

Al-Ragum, A., Monge-Ganuzas, M., Amos, C. L., Cearreta, A., Townend, I., & Manca, E. (2014). An evaluation of the Rouse theory for sand transport in the Oka estuary, Spain. Continental Shelf Research, 78, 39-50.

Amos, C. L., Kassem, H., Townend, I., Umgiesser, G., Madricardo, F., Zaggia, L., Manfe, G., Lorenzetti, G., & Gomez, E. (2020). Using historical data to examine the accuracy of sand transport field measurements in two nearshore marine settings. Journal of Coastal Research, 36(5), 1013-1028.

Benito, I., & Onaindia, M. (1991). Estudio de la distribución de las plantas halófitas y su relación con los factores ambientales en la marisma de Mundaka-Urdaibai. Implicaciones en la gestión del Medio Ambiente. Eusko Ikaskuntza. Sociedad de Estudios Vascos. Cuadernos de la sección Ciencias Naturales (8).

Camus, P., Losada, I. J., Izaguirre, C., Espejo, A., Menéndez, M., & Pérez, J. (2017). Statistical wave climate projections for coastal impact assessments. Earth's Future, 5(9), 918-933.

Cearreta, A., Irabien, M. J., Ulibarri, I., Yusta, I., Croudace, I. W., & Cundy, A. B. (2002). Recent salt marsh development and natural regeneration of reclaimed areas in the Plentzia estuary, N. Spain. Estuarine, Coastal and Shelf Science, 54(5), 863-886.

1011 Cearreta, A. & Monge-Ganuzas, M. (2013). Evolución paleoambiental del estuario del
1012 Oka (Reserva de la Biosfera de Urdaibai, Vizcaya): respuesta al ascenso del
1013 nivel marino durante el Holoceno. Geo-Temas, 14, 163-166

1014 Cearreta, A., García-Artola, A., Leorri, E., Irabien, M. J., & Masque, P. (2013). Recent
1015 environmental evolution of regenerated salt marshes in the southern Bay of
1016 Biscay: anthropogenic evidences in their sedimentary record. Journal of Marine
1017 Systems, 109, S203-S212.

1018 Chust, G., Caballero, A., Marcos, M., Liria, P., Hernández, C., & Borja, Á. (2010).
1019 Regional scenarios of sea level rise and impacts on Basque (Bay of Biscay)
1020 coastal habitats, throughout the 21st century. Estuarine, Coastal and Shelf
1021 Science, 87(1), 113-124.

1022 Chust, G., Á. Borja, A. del Campo, P. Liria, J. Franco, I. Muxika, R. Roa, J. G.
1023 Rodríguez, Joxe M. Garmendia (2013). Inundabilidad de los estuarios y costa de
1024 Bizkaia por ascenso del nivel del mar mediante LiDAR topográfico y
1025 batimétrico: cartografía y evaluación de impactos. Report made by AZTI-
1026 Tecnalia for URA (Uraren Euskal Agentzia), 37 pp.
1027 https://www.uragentzia.euskadi.eus/informe_estudio/inundabilidad-de-los-
1028 estuarios-y-costa-de-bizkaia-por-ascenso-del-nivel-del-mar-mediante-lidar-
1029 topografico-y-batimetrico-cartografia-y-evaluacion-de-impactos/webura00-
1030 contents/es/

1031 Chust, G., González, M., Fontán, A., Revilla, M., Alvarez, P., Santos, M., Cotano, U.,
1032 Chifflet, M., Borja, A., Muxika, I., Sagarminaga, Y., Caballero, A., de Santiago,
1033 I., Epelde, I., Liria, P., Ibaibarriaga, L., Garnier, R., Franco, J., Villarino, E.,
1034 Irigoien, X., Fernandes-Salvador, J.A., Uriarte, A., Esteban, X., Orue-
1035 Echevarria, D., Figueira, T. & Uriarte, A. (2022). Climate regime shifts and

biodiversity redistribution in the Bay of Biscay. Science of The Total Environment, 803, 149622.

Coco, G., Zhou, Z., Van Maanen, B., Olabarrieta, M., Tinoco, R., & Townend, I. (2013). Morphodynamics of tidal networks: Advances and challenges. Marine Geology, 346, 1-16.

Dam G, van der Wegen M, Labeur R J and Roelvink D (2016). Modeling centuries of estuarine morphodynamics in the Western Scheldt estuary. Geophysical Research Letters, 10.1002/2015gl066725.

del Campo, A., González, M., Uriarte, A., Castillo, C. & de Santiago, I. (2021). A socio-economic assessment of the sea-level rise on the Basque Coast municipalities (NW coast of Spain) due to the climate change. Arias, A., Ríos, P., Paxton, H.,Sánchez, O., Acuña, J. L., Álvarez, A., Manjón-Cabeza, M. E. & Cristobo, J. (Eds). 2021. Proceedings of the XVII In-ternational Symposium on Oceanography of the Bay of Biscay (ISOBAY 17). University of Oviedo, 134 pp.

Dennis, J. M., Spearman, J. R., & Dearnaley, M. P. (2000). The development of a regime model for prediction of the long-term effects of civil engineering activities on estuaries. Physics and Chemistry of the Earth, Part B: Hydrology, Oceans and Atmosphere, 25(1), 45-50.

Elliott M, Day J W, Ramachandran R and Wolanski E. (2019). Chapter 1 - A Synthesis: What Is the Future for Coasts, Estuaries, Deltas and Other Transitional Habitats in 2050 and Beyond?, In: Coasts and Estuaries, Series, Wolanski E, Day J W, Elliott M and Ramachandran R (eds), pp. 1-28, Elsevier.

Fox-Kemper, B., H. T. Hewitt, C. Xiao, G. Aðalgeirsdóttir, S. S. Drijfhout, T. L. Edwards, N. R. Golledge, M. Hemer, R. E. Kopp, G. Krinner, A. Mix, D. Notz, S. Nowicki, I. S. Nurhati, L. Ruiz, J-B. Sallée, A. B. A. Slangen, Y. Yu (2021). Ocean, Cryosphere and Sea Level Change. In: Climate Change 2021: The Physical Science Basis. Contribution of Working Group I to the Sixth Assessment Report of the Intergovernmental Panel on Climate Change [Masson-Delmotte, V., P. Zhai, A. Pirani, S. L. Connors, C. Péan, S. Berger, N. Caud, Y. Chen, L. Goldfarb, M. I. Gomis, M. Huang, K. Leitzell, E. Lonnoy, J.B.R. Matthews, T. K. Maycock, T. Waterfield, O. Yelekçi, R. Yu and B. Zhou (eds.)]. Cambridge University Press. In Press.

French, J. R., & Burningham, H. (2003). Tidal marsh sedimentation versus sea-level rise: a southeast England estuarine perspective. In Proceedings Coastal Sediments (Vol. 3, pp. 1-14).

French J, Payo A, Murray B, Orford J, Eliot M and Cowell P (2016). Appropriate complexity for the prediction of coastal and estuarine geomorphic behaviour at decadal to centennial scales. Geomorphology, 256, 3-16.

Gainza, J., Garnier, R., Nunez, P., Jaramillo, C., González, E.M., Medina, R., Liria, P., Epelde, I., Uriarte, A. & Monge-Ganuzas, M. (2019). Accelerating Beach Recovery by Plowing the Intertidal Bar: A Field Experiment along the Northern Spanish Coast. J. Coast. Res., 35(5), pp.973-984

García-Artola, A. (2013). Geological record of the recent anthropogenic impact on salt marshes from the Eastern Cantabrian coast: agricultural occupation, environmental regeneration and response to climate change (PhD Dissertation). University of the Basque Country.

García-Artola, A., Cearreta, A., & Leorri, E. (2015). Relative sea-level changes in the Basque coast (northern Spain, Bay of Biscay) during the Holocene and Anthropocene: The Urdaibai estuary case. Quaternary International, 364, 172-180.

García-Artola, A., Stéphan, P., Cearreta, A., Kopp, R. E., Khan, N. S., & Horton, B. P. (2018). Holocene sea-level database from the Atlantic coast of Europe. Quaternary Science Reviews, 196, 177-192.

Hall J W, Harvey H and Manning L J. (2019). Adaptation thresholds and pathways for tidal flood risk management in London. Climate Risk Management, 24, 42-58.

Halpern, B. S., Frazier, M., Afflerbach, J., Lowndes, J. S., Micheli, F., O'Hara, C., Scarborough, C. & Selkoe, K. A. (2019). Recent pace of change in human impact on the world's ocean. Scientific reports, 9(1), 1-8.

IPBES (2019): Summary for policymakers of the global assessment report on biodiversity and ecosystem services of the Intergovernmental Science-Policy Platform on Biodiversity and Ecosystem Services. S. Díaz, J. Settele, E. S. Brondízio, H. T. Ngo, M. Guèze, J. Agard, A. Arneth, P. Balvanera, K. A. Brauman, S. H. M. Butchart, K. M. A. Chan, L. A. Garibaldi, K. Ichii, J. Liu, S. M. Subramanian, G. F. Midgley, P. Miloslavich, Z. Molnár, D. Obura, A. Pfaff, S. Polasky, A. Purvis, J. Razzaque, B. Reyers, R. Roy Chowdhury, Y. J. Shin, I. J. Visseren-Hamakers, K. J. Willis, and C. N. Zayas (eds.). IPBES secretariat, Bonn, Germany. 56 pages.

IPCC (2021): Summary for Policymakers. In: Climate Change 2021: The Physical Science Basis. Contribution of Working Group I to the Sixth Assessment Report of the Intergovernmental Panel on Climate Change [Masson-Delmotte, V., P.

Zhai, A. Pirani, S.L. Connors, C. Péan, S. Berger, N. Caud, Y. Chen, L. Goldfarb, M.I. Gomis, M. Huang, K. Leitzell, E. Lonnoy, J.B.R. Matthews, T.K. Maycock, T. Waterfield, O. Yelekçi, R. Yu, and B. Zhou (eds.)]. In Press.

Knaapen, M., Townend, I., Rossington, K., Fletcher, C. A., & Spearman, J. (2009). Modelling the dynamics of intertidal mudflat and salt marshes within estuaries. The Environmentalist, (84), 12-15.

Larsen L G, Eppinga M B, Passalacqua P, Getz W M, Rose K A and Liang M. (2016). Appropriate complexity landscape modeling. Earth-Science Reviews, 160, 111-130, 10.1016/j.earscirev.2016.06.016.

Lesser, G.R., Roelvink, J.A., Van Kester, J.A.T.M., Stelling, G.S., 2004. Development and validation of a three-dimensional morphological model. Coast. Eng. 51, 883–915.Liria, P., Garel, E., & Uriarte, A. (2009). The effects of dredging operations on the hydrodynamics of an ebb tidal delta: Oka Estuary, northern Spain. Continental Shelf Research, 29(16), 1983-1994.

Liria, P., Garel, E., & Uriarte, A. (2009). The effects of dredging operations on the hydrodynamics of an ebb tidal delta: Oka Estuary, northern Spain. Continental Shelf Research, 29(16), 1983-1994.

Liria, P., Epelde, I., de Santiago, I., Garnier, R., Abalia, A., Mader, J. (2021). KOSTASystem, a coastal videometry technology: development and applications. EuroGOOS International Conference, 3-5 May 2021.

Monge-Ganuzas, M., Cearreta, A., & Iriarte Avilés, E. (2008). Consequences of estuarine sand dredging and dumping on the Urdaibai Reserve of the Biosphere (Bay of Biscay): the case of the “Mundaka left wave”, Journal of Iberian Geology, 34 (2), 215-234.

1131 Monge-Ganuzas, M., Cearreta, A., & Evans, G. (2013). Morphodynamic consequences
1132 of dredging and dumping activities along the lower Oka estuary (Urdaibai
1133 Biosphere Reserve, southeastern Bay of Biscay, Spain). Ocean & coastal
1134 management, 77, 40-49.

1135 Monge-Ganuzas, M., Evans, G., & Cearreta, A. (2015). Sand-spit accumulations at the
1136 mouths of the eastern Cantabrian estuaries: The example of the Oka estuary
1137 (Urdaibai Biosphere Reserve). Quaternary International, 364, 206-216.

1138 Monge-Ganuzas M, Gainza J, Liria P, Epelde I, Uriarte A, Garnier R, González M,
1139 Nuñez P, Jaramillo C & Medina R (2017). Morphodynamic evolution of Laida
1140 beach (Oka estuary, Urdaibai Biosphere Reserve, southeastern Bay of Biscay) in
1141 response to supratidal beach nourishment actions. Journal of Sea Research, 130,
1142 85-95.

1143 Monge-Ganuzas, M., Cearreta, A., Irabién, M.J., García-Artola, A. (2019). Estuaries of
1144 the Basque Coast. In: Morales J. (eds) The Spanish Coastal Systems. Springer,
1145 437-465.

1146 Morris, J. T., Sundareshwar, P. V., Nietch, C. T., Kjerfve, B., & Cahoon, D. R. (2002).
1147 Responses of coastal wetlands to rising sea level. Ecology, 83(10), 2869-2877.

1148 Murray, A.B. (2007). Reducing model complexity for explanation and prediction.
1149 Geomorphology, 90 (3-4), 178-191.

1150 Murray, A.B. (2013). Which Models Are Good (Enough), and When?, In: Quantitative
1151 Modeling of Geomorphology, Series: Treatise on Geomorphology, Vol 2, Baas
1152 A C W (ed), pp. 50-58, Academic Press, San Diego.

1153 Pontee, N. (2017). Dispelling the myths surrounding coastal squeeze. In Flood and
1154 Coast 2017 conference. International Centre, Telford (pp. 28-30).

1155 Prego, R., Boi, P., & Cobelo-García, A. (2008). The contribution of total suspended
1156 solids to the Bay of Biscay by Cantabrian Rivers (northern coast of the Iberian
1157 Peninsula). Journal of Marine Systems, 72(1-4), 342-349.

1158 Peraza-Castro, M., Ruiz-Romera, E., Montoya-Armenta, L. H., Sánchez-Pérez, J. M., &
1159 Sauvage, S. (2015). Evaluation of hydrology, suspended sediment and Nickel
1160 loads in a small watershed in Basque Country (Northern Spain) using eco-
1161 hydrological SWAT model. In Annales de Limnologie-International Journal of
1162 Limnology (Vol. 51, No. 1, pp. 59-70). EDP Sciences.

1163 Peraza-Castro, M., Ruiz-Romera, E., Meaurio, M., Sauvage, S., & Sánchez-Pérez, J. M.
1164 (2018). Modelling the impact of climate and land cover change on hydrology
1165 and water quality in a forest watershed in the Basque Country (Northern Spain).
1166 Ecological Engineering, 122, 315-326.

1167 Rees J G. (2006). Sea-level, topographical and sediment supply controls on Holocene
1168 sediment composition in the Humber Estuary. Phil.Trans.R.Soc.Lond.A., 364,
1169 993-1008.

1170 Reiblich, J., Hartge, E., Wedding, L.M., Killian, S., Verutes, G.M. 2019. Bridging
1171 climate science, law, and policy to advance coastal adaptation planning, Mar.
1172 Pol. 104, 125–134.

1173 Roelvink, J. A., & Van Banning, G. K. F. M. (1995). Design and development of
1174 DELFT3D and application to coastal morphodynamics. Oceanographic
1175 Literature Review, 11(42), 925.

1176 Roelvink D and Reniers A. (2012). A guide to modelling coastal morphology, World
1177 Scientific Publishing, Singapore.

1178 Rossington, S. K., Nicholls, R. J., Stive, M. J. F., & Wang, Z. B. (2011). Estuary
1179 schematisation in behaviour-oriented modelling. Marine Geology, 281(1-4), 27-
1180 34.

1181 Sainz de Murieta, E. (2016). Environmental and economic impacts of sea-level rise on
1182 the Basque Coast (Doctoral dissertation, Universidad del País Vasco-Euskal
1183 Herriko Unibertsitatea).

1184 Scully M E and Friedrichs C T (2007), Sediment pumping by tidal asymmetry in a
1185 partially mixed estuary. Journal of Geophysical Research, 112 (C07028).

1186 Shaxson L. (2005), Is your evidence robust enough? Questions for policy makers and
1187 practitioners. Evidence & Policy: A Journal of Research, Debate and Practice, 1
1188 (1), 101-112, https://doi.org/10.1332/1744264052703177.

1189 Stive, M. J. F., Capobianco, M., Wang, Z. B., Ruol, P. & Buijsman, M. C. (1998).
1190 Morphodynamics of a tidal lagoon and adjacent coast. In: Dronkers, J.,
1191 Scheffers, M.B.A.M., eds., Proceedings of the 8th International Biennial
1192 Conference on Physics of Estuaries and Coastal Seas. A.A. Balkema, pp. 397-
1193 407.

1194 Townend, I. H. (2004). Identifying change in estuaries. Journal of Coastal Conservation,
1195 10, 5-12.

1196 Townend, I. H., Wang, Z. B., & Rees, J. G. (2007). Millennial to annual volume
1197 changes in the Humber Estuary. Proceedings of the Royal Society A:
1198 Mathematical, Physical and Engineering Sciences, 463(2079), 837-854.

1199 Townend, I. H., Wang, Z. B., Stive, M., & Zhou, Z. (2016a). Development and
1200 extension of an aggregated scale model: Part 1 – Background to ASMITA.
1201 China Ocean Engineering, 30(4), 483-504.

Townend, I., Wang, Z. B., Stive, M., & Zhou, Z. (2016b). Development and extension of an aggregated scale model: Part 2 – Extensions to ASMITA. China Ocean Engineering, 30(5), 651-670.

Townend, I. H., 2021, ASMITA OO manual, Version 1.5, CoastalSEA, UK, pp44, www.coastalsea.uk.

Townend, I., Zhou, Z., Guo, L., & Coco, G. (2021). A morphological investigation of marine transgression in estuaries. Earth Surface Processes and Landforms, 46(3), 626-641.

Townend I H, French J R, Nicholls R J, Brown S, Carpenter S, Haigh I D, Hill C T, Lazarus E, Penning-Rowsell E C, Thompson C E L and Tompkins E L (2021), Operationalising coastal resilience to flood and erosion hazard: A demonstration for England. Science of The Total Environment, 783, https://doi.org/10.1016/j.scitotenv.2021.146880.

Valle, M., Chust, G., del Campo, A., Wisz, M. S., Olsen, S. M., Garmendia, J. M., & Borja, Á. (2014). Projecting future distribution of the seagrass *Zostera noltii* under global warming and sea level rise. Biological Conservation, 170, 74-85.

Valle, M., Pala, V., Lafon, V., Dehouck, A., Garmendia, J. M., Borja, A., & Chust, G. (2015). Mapping estuarine habitats using airborne hyperspectral imagery, with special focus on seagrass meadows. Estuarine, Coastal and Shelf Science, 164, 433-442.

van der Wegen M and Roelvink J A (2012). Reproduction of estuarine bathymetry by means of a process-based model: Western Scheldt case study, the Netherlands. Geomorphology, 179 (0), 152-167.

van Goor M A, Zitman T J, Wang Z B and Stive M J F (2003). Impact of sea-level rise on the morphological equilibrium state of tidal inlets. Marine Geology, 202, 211-227, https://doi.org/10.1016/s0025-3227(03)00262-7.

van Maanen B, Nicholls R J, French J R, Barkwith A, Bonaldo D, Burningham H, Brad Murray A, Payo A, Sutherland J, Thornhill G, Townend I H, van der Wegen M and Walkden M J A. (2016). Simulating mesoscale coastal evolution for decadal coastal management: A new framework integrating multiple, complementary modelling approaches. Geomorphology, 256, 68-80, 10.1016/j.geomorph.2015.10.026.

Wang, Z. B., De Vriend, H. J., Stive, M. J., Townend, I. H., Dohmen-Jansen, C. M., & Hulscher, S. J. M. H. (2008). On the parameter setting of semi-empirical long-term morphological models for estuaries and tidal lagoons.

Wang, Z. B., & Townend, I. H. (2012). Influence of the nodal tide on the morphological response of estuaries. Marine Geology, 291, 73-82.

Wang, Z. B., Townend, I., & Stive, M. (2020). Aggregated morphodynamic modelling of tidal inlets and estuaries. Water Science and Engineering, 13(1),1-3.

Wong, P.P., Losada, I.J., Gattusso, J.P., Hinkel, J., Khattabi, A., McInnes, K., Saito, Y., Sallenger, A., (2014). Coastal systems and low-lying areas. Climate change, 2104, 361-409.